remote sensing

MDPI

Article

Validation of MODIS C6 Dark Target Aerosol Products at 3 km and 10 km Spatial Resolutions Over the China Seas and the Eastern Indian Ocean

Xiaojing Shen [1], Muhammad Bilal [2], Zhongfeng Qiu [2,*], Deyong Sun [2], Shengqiang Wang [2] and Weijun Zhu [2]

[1] School of Atmospheric Sciences, Nanjing University of Information Science & Technology, Nanjing 2100444, China; ShenXJ@nuist.edu.cn

[2] School of Marine Sciences, Nanjing University of Information Science & Technology, Nanjing 2100444, China; muhammad.bilal@connect.polyu.hk (M.B.); sundeyong1984@163.com (D.S.); wsqiang815@163.com (S.W.); weijun@nuist.edu.cn (W.Z.)

* Correspondence: zhongfeng.qiu@nuist.edu.cn; Tel.: +86-25-5869-5696

Received: 24 February 2018; Accepted: 4 April 2018; Published: 8 April 2018



Abstract: In this study, MODerate resolution Imaging Spectroradiometer (MODIS) Collection 6 (C6) level-2 Dark Target (DT) Aerosol Optical Depth (AOD) products at 3 km (DT3K) and 10 km (DT10K) spatial resolutions were validated over the China seas and the eastern Indian Ocean against Maritime Aerosol Network (MAN) Level 1.5 AOD measurements collected through 13 cruises from 2010 to 2014. For this, DT3K and DT10K AOD observations were obtained from four Scientific Data Sets (SDS), i.e., "Effective_Optical_Depth_Average_Ocean" ($EODAO_{AOD}$), "Effective_Optical_Depth_Best_Ocean" ($EODBO_{AOD}$), "Image_Optical_Depth_Land_And_Ocean" ($IODLAO_{AOD}$) and "Optical_Depth_Land_And_Ocean" ($ODLAO_{AOD}$). The MAN AOD measurements were filtered within (i) ±2 h, (ii) ±4 h, (iii) ±6 h, and (iv) ±12 h of MODIS overpass time. Results showed that the DT10K and DT3K performed equally over the China seas and the eastern Indian Ocean in terms of retrievals quality and agreement with the MAN AOD measurements, whereas the DT3K has less coincident observations than the DT10K. For seasonal analysis, larger underestimation in the DT algorithm was observed in autumn followed by spring, whereas retrievals were well correlated with the MAN AOD data in summer. Overall, this study found that $ODLAO_{AOD}$ observations for the DT3K and DT10K were much better than $EODAO_{AOD}$, $EODBO_{AOD}$ and $IODLAO_{AOD}$ in terms of high correlation and a large percentage of the AOD retrievals within the Expected Error (EE = +(0.04 + 10%), −(0.02 + 10%)).

Keywords: MODIS; AOD; Validation; DT; MAN

1. Introduction

Aerosols are important components of the Earth's climate system and play an important role in the global energy budget [1], perturbing the hydrological cycle [2], and reducing atmospheric visibility [3], and in large concentrations are harmful to human health [4]. The particles travel from one place to another and accumulate in the atmosphere over periods of days and weeks [5]. Aerosol effects on weather and air quality are uncertain, due to lack of understanding of spatiotemporal variations in their optical properties. Therefore, characterizing aerosol spatial variations and distributions over time are necessary for understanding the present and possible future climate conditions. For this, ground-based Sun photometers such as Aerosol Robotic Network (AERONET) [6,7] over land and Maritime Aerosol Network (MAN) [8,9] over the ocean are used to provide multispectral aerosol properties including aerosol optical depth (AOD) at high temporal resolution but over limited locations.

The spatial limitation of ground monitoring stations is overcome by space-borne technology which provides a near-real-time global view of aerosol optical properties at low to high spatial resolutions. Aerosol optical properties can be obtained from different sensors such as the Polarization and Directionality of the Earth's Reflectances (POLDER) [10], the Total Ozone Mapping Spectrometer (TOMS) [11], the Along Track Scanning Radiometer (ATSR-2) [12], the Ozone Monitoring Instrument (OMI) [13], the Geostationary Operational Environmental Satellite (GOES) [14], the Seaviewing Wide Field-of-view Sensor (SEAWIFS) [15], the Multiangle Imaging Spectroradiometer (MISR) [16,17], the Advanced Very High Resolution Radiometer (AVHRR) [18,19], the Medium Resolution Imaging Spectroradiometer (MERIS) [20], and AOD is available as a standard product from the MODIS (deep blue algorithm [21–24] and dark target algorithm [25–30].

MODIS sensors have been flying in polar orbits on Terra since 2000 and Aqua since 2002 [31] to provide geophysical data of Earth. MODIS has a wide spectral range of 0.41 μm to 14.5 μm in 36 channels, a broad swath of 2330 km and spatial resolution of 250 m to 1 km depending on the channel. It provides global AOD products over land based on the Dark Target (DT) and Deep Blue (DB) algorithms [21,22,26,32], and over ocean based on the DT ocean algorithm at a 10 km spatial resolution. Previous studies reported that 10 km resolution is not fine enough to resolve local variability [33–40]. Therefore, a Collection (C6) of MODIS aerosol products include aerosol observations over land and ocean at a 3 km resolution based on the DT algorithm in addition to 10 km [41,42]. Previous studies found that the DT3K AOD product has similar or more uncertainties over land and ocean compared to the DT10K [34,39,42–45].

The MODIS C6 DT aerosol algorithms, well documented in the literature [32,46–49], provide global AOD products at 3 km and 10 km resolutions. The DT aerosol algorithm inputs consist of calibrated radiances normalized to reflectance in 7 wavelengths, total column ozone concentrations from the NOAA Office of Satellite Product Operations, total column precipitable water vapor from the National Center for Environmental Prediction (NCEP) reanalysis, the MODIS cloud mask (MOD/MYD35), and surface wind speed from NCEP, using Look–Up–Table (LUT) and estimated surface estimation to retrieve AOD over ocean [41,42]. For AOD retrieval, the entire MODIS granule is organized into retrieval boxes of 6 × 6 pixels for DT3K and 20 × 20 pixels for DT10K. The DT ocean algorithm uses spatial variability, ratio and threshold tests [50–53] to mask cloud contaminated pixels, spectral tests [50,54] to identify and mask sediments, and a 40° static sun glint mask to remove glint affected pixels from the retrieval box. The remaining pixels are sorted based on their lowest to highest near-infrared reflectance (0.86 μm), and among them, the darkest 25% and brightest 25% pixels are deselected to avoid residual cloud and surface contamination [43,48]. Once these darkest and brightest pixels are discarded, the algorithm averages the remaining pixels to represent conditions in the 3 km retrieval box. The DT3K ocean algorithm requires a minimum of 5 pixels at 0.86 μm over the ocean with at least 12 pixels distributed over the other five channels to continue and make a retrieval. This is a more stringent requirement for DT3K over the ocean (14% of 36) than DT10K (2.5%) for the best quality retrievals [42]. The DT AOD over ocean is reported for seven channels (0.47, 0.55, 0.65, 0.86, 1.24, 1.63, and 2.11 μm) and ocean retrievals are valid for non-zero Quality Flags (QF > 0). The expected error (EE) of the C6 DT AOD over ocean is (+(0.04 + 10%), −(0.02 + 10%)) [41].

High-resolution AOD observations are required for monitoring atmospheric aerosols over complex water surface at a local scale. Only a few studies are available for validation of the DT3K and DT10K AOD observations over water at local to global scales [41,43]. Most of the times in a year, the atmosphere over the China seas and the eastern Indian Ocean is contaminated by aerosol particles, and validation studies of the MODIS aerosol products are limited to understand aerosol variations and their effects over the China seas and the eastern Indian Ocean. Therefore, the main objective of this study is to validate the MODIS DT3K and DT10K AOD products and highlight their capabilities for aerosol monitoring and mapping over the region.

2. Study Area and Data Set

2.1. Study Area

The combined waterbody of China seas and the eastern Indian Ocean, together, with a maximum depth greater than 5000 m, is the largest marginal sea in Southeast Asia. It extends from the equator to 23°N and from 99°E to 121°E and joins the Pacific Ocean through the Luzon Strait between the Taiwan Island and the Luzon Island [55]. It is bounded in the north by the passive south China continental margin. To the south, small continental blocks that were drifted off mainland Asia, separate the basin from an extinct subduction zone along Palawan and northwest Borneo. The combined waterbody of China seas and the eastern Indian Ocean has an area of 3.3 million km^2 excluding the Gulfs of Thailand and Tonkin [56]. There are great differences in water type and quality over the region as turbidity of the coastal water is higher than deep ocean water [57].

2.2. MAN AOD

The Maritime Aerosol Network constitutes a component of the AERONET is affiliated with the AERONET calibration and data processing standards and procedures [7]. The proposed activity involved handheld Sun photometer measurements from various ships (scientific and non-scientific) and will complement island-based AERONET measurements, thus extending data collection to the vast regions where no islands exist [8]. The direct Sun measurements are acquired in five spectral channels within the spectral range between 340 nm and 1020 nm. The estimated uncertainty of the optical depth in each channel does not exceed ±0.02 [58], primarily due to inter-calibration against AERONET CIMEL instruments which are more accurate, i.e., uncertainty within 0.01 in the visible and near-infrared channels [59]. Thus, MAN provides high-quality AOD measurements with known uncertainty. In this study, MAN L1.5 AOD data from 13 different cruises (represented by different color symbols in Figure 1, and Table 1) are obtained for validation of the DT3K and DT10K AOD products.

Table 1. Summary of the MAN AOD data used in this study.

Cruise	N	Latitude		Longitude		Year
		Min	Max	Min	Max	
Eardo_13	6	33.004	34.321	126.479	126.759	September 2013–October 2013
Marion_Dufresne_10_2	57	8.943	43.195	111.502	141.015	May 2010–June 2010
RV_1_2010	19	18	22.404	115.657	120.057	March 2010
Shiyan_11_0	104	−5.08	22.138	79.811	113.788	April 2011–May 2011
Shiyan_12_0	297	−5.002	19.756	79.839	113.513	February2012–April 2012
Shiyan_12_1	263	13.963	21.827	110.249	118.986	October 2012
Shiyan_13_0	314	1.533	21.837	83.804	113.86	April 2013–May 2013
Shiyan_13_1	132	14.849	22.665	110.908	120.006	September 2013–October2013
Shiyan_14_0	254	−6.203	19.975	101.307	113.127	March 2014–April2014
Shiyan_14_1	235	5.827	19.067	84.591	110.957	May 2014
Vasco_11	180	11.75	14.5	120.217	120.8	September 2011
Vasco_12	55	7.85	12.683	116.933	120.467	September 2012
Zim_San_Diego_10	145	1.675	51.161	−173.342	164.766	July 2012–August 2010

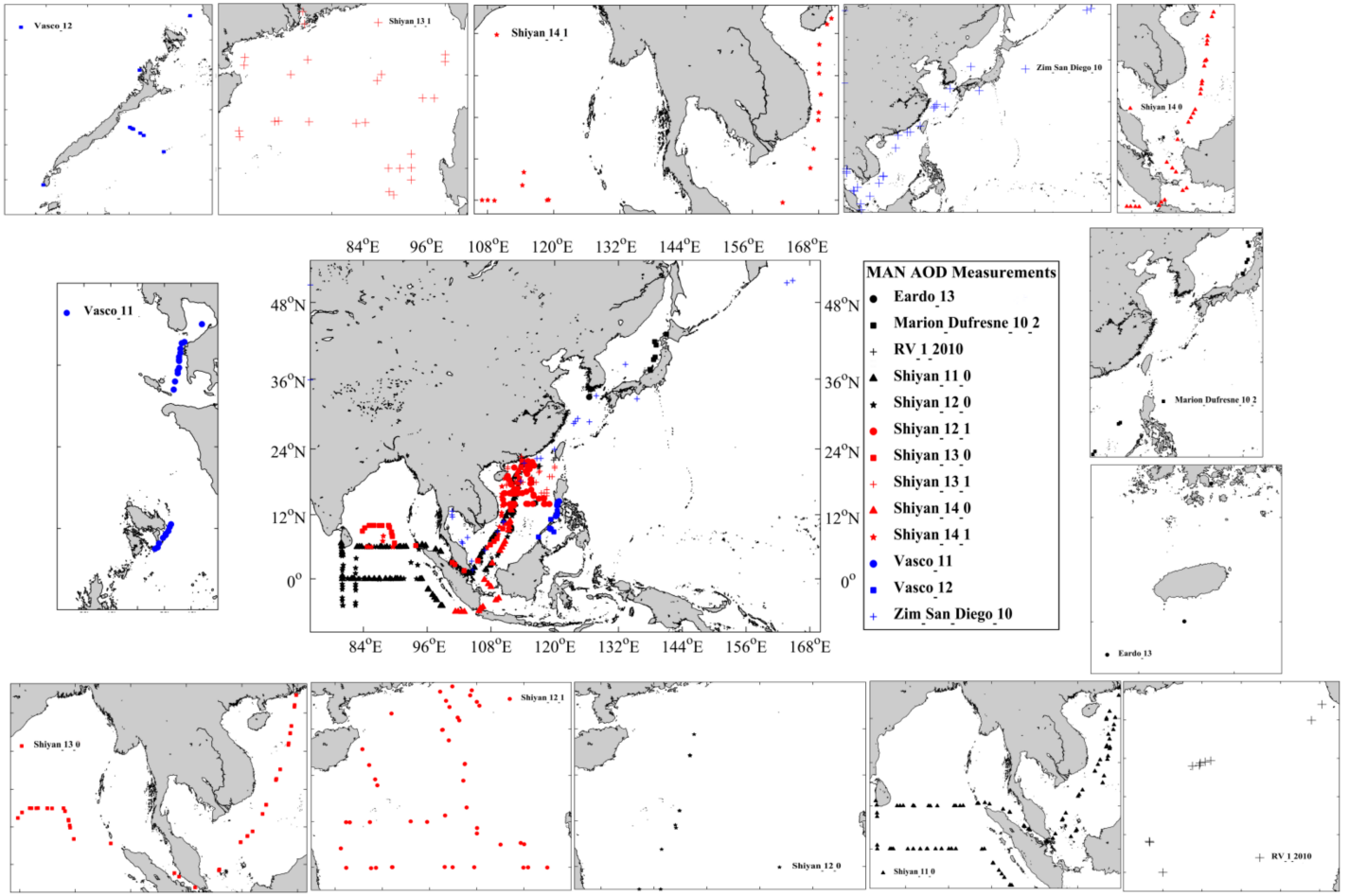


Figure 1. Locations of MAN AOD measurements collected through 13 different cruises, and different colors and symbols represent sampling sites.

2.3. MODIS Dataset

In this study, Aqua-MODIS C6 level-2 operational DT3K and DT10K aerosol products (MYD04) were downloaded from the "Level-1 and Atmosphere Archive and Distribution System (LAADS) Distributed Active Archive Center (DAAC)" (https://ladsweb.nascom.nasa.gov/) to obtain the DT AOD retrievals for validation. The MODIS daily level-3 Remote Sensing Reflectance (Rrs) product at 4 km resolution was downloaded from (https://oceandata.sci.gsfc.nasa.gov/MODIS-Aqua/Mapped/Daily/4km/Rrs/) to match with MAN AOD and MODIS AOD. Table 2 gives a detailed summary of the dataset used in this study.

Table 2. Summary of the dataset used in the current study from 2010 to 2014.

Data	Scientific Data Set (SDS) Name	Contents
MYD04	Effective_Optical_Depth_Average_Ocean Effective_Optical_Depth_Best_Ocean Image_Optical_Depth_Land_And_Ocean Optical_Depth_Land_And_Ocean	DT3K and DT10K over the ocean
MODIS A	Remote Sensing Reflectance	Daily Rrs at 4 km
MAN	Level 1.5	AOD

3. Methods

In this study, Aqua-MODIS C6 DT3K and DT10K aerosol products were obtained for the China seas and the eastern Indian Ocean according to the time period of available ground data collected by 13 different cruises from 2010 to 2014. Only those DT3K and DT10K AOD retrievals at 0.55 μm passing recommended quality flags (QF) checks [41] were used for validation. The DT3K and DT10K AOD retrievals were obtained from the SDS (i) "Effective_Optical_Depth_Average_Ocean", i.e., retrieved $EODAO_{AOD}$ over water for "average" solution at seven channels; (ii) "Effective_Optical_Depth_Best_Ocean", i.e., retrieved $EODBO_{AOD}$ over water for "best" solution at seven channels; (iii) "Image_Optical_Depth_Land_And_Ocean", i.e., retrieved $IODLAO_{AOD}$ over water for "average" solution (QF = 1, 2, 3) and over land for all quality flags (QF = 0, 1, 2, 3) at 0. 55 μm; and (iv) "Optical_Depth_Land_And_Ocean", i.e., retrieved $ODLAO_{AOD}$ over water for "average" solution (QF = 1, 2, 3) and over land for "best" (QF = 3). More information about each SDS can be found in [41]. The AOD observations from each SDS were used same as available except for the SDS "Optical_Depth_Land_And_Ocean", for which $ODLAO_{AOD}$ was filtered for the highest quality assurance flag (QF = 3) using the SDS "Land_Ocean_Quality_Flag". In other words, the DT3K and DT10K AOD observations were used from "average" to "best" solutions for validation. As MAN does not provide AOD measurements at 0.55 μm, the MAN AOD was interpolated to 0.55 μm using Ångström exponent (α) (Equations (1) and (2)) to match with the MODIS AOD:

$$\alpha = -\frac{\ln \frac{\tau_{\lambda_1}}{\tau_{\lambda_2}}}{\ln \frac{\lambda_1}{\lambda_2}} \quad (1)$$

$$\frac{\tau_\lambda}{\tau_{\lambda_0}} = \left(\frac{\lambda}{\lambda_0}\right)^{-\alpha} \quad (2)$$

where, α is Ångström exponent, and λ is the wavelength.

To consider the atmospheric variability and increase the number of samples, the MAN AOD measurements were considered within (i) ±2 h; (ii) ±4 h; (iii) ±6 h; and (iv) ±12 h of MODIS over pass time for each sampling site, and an average of at least two pixels of MODIS AOD observations within a sampling window of 3 × 3 pixels (average of 9 pixels) centered on the MAN AOD location, i.e., average of 9 km × 9 km region for the DT3K, and 30 km × 30 km region for the DT10K,

was considered. The coincident AOD observations for $EODAO_{AOD}$ were 397 for DT3K and 697 for DT10K, for $EODBO_{AOD}$ were 397 for DT3K and 697 for DT10K, for $IODLAO_{AOD}$ were 419 for DT3K and 730 for DT10K, and for $ODLAO_{AOD}$ were 272 for DT3K and 512 for DT10K. Unavailability of the satellite AOD observations corresponding to MAN AOD was due to the limitation of the aerosol algorithm, data collection gaps and cloud cover [43].

Four statistical indicators such as correlation coefficient (R), root mean square error (RMSE), mean absolute error (MAE), and expected error (EE) of AOD were used to evaluate MODIS AOD against MAN AOD. The correlation coefficient (R) is a dimensionless index, which is invariant to linear transformations of either variable [60]. It indicates agreement between the MODIS AOD and the MAN AOD, and the higher values the better agreement. In this study, R is obtained from Deming Regression (DR) instead of that from Linear Regression (LR) because DR estimates an unbiased slope by assuming the Gaussian distribution of errors in both x and y data points (which is typical of our data) [61–63]. While LR estimates a biased slope by assuming random measurement errors in the dependent variable (y) and an error-free independent variable (x) [61,64–66], but is inappropriate for use when significant errors are expected in both variables.

The root mean square error (RMSE) was used to measure the differences between MODIS and MAN AOD which is sensitive to both systematic and random errors. The equation to calculate RMSE is as follow:

$$RMSE = \sqrt{\frac{1}{n}\sum_{i=1}^{n}(AOD_{MODISi} - AOD_{MANi})^2} \quad (3)$$

The mean absolute error (MAE) is the most natural measure of mean error magnitude [67] and calculated as Equation (4):

$$MAE = \frac{1}{n}\sum_{i=1}^{n}|AOD_{MODISi} - AOD_{MANi}| \quad (4)$$

Expected error (EE) is estimated for the uncertainty of MODIS AOD over ocean [41].

$$EE = (+(0.04 + 0.10 \times AOD_{MAN}), -(0.02 + 0.10 \times AOD_{MAN})) \quad (5)$$

The MODIS AOD retrievals were reported as a good quality if they fall within the following envelope (Equation (6)).

$$AOD_{MAN} - |-EE| \leq AOD_{MODIS} \leq AOD_{MAN} + |+EE| \quad (6)$$

4. Results and Discussions

4.1. Validation of MODIS DT Ocean Algorithm

4.1.1. Validation of DT AOD at 10 km Resolution

Figure 2 shows the validation of the DT10K $EODAO_{AOD}$ (Figure 2a–d), $EODBO_{AOD}$ (Figure 2e–h), $IODLAO_{AOD}$ (Figure 2i–l), and $ODLAO_{AOD}$ observations (Figure 2m–p) against MAN AOD measurements over the China seas and the eastern Indian Ocean for different time intervals, i.e., within ±2 h (Figure 2a,e,i,m), ±4 h (Figure 2b,f,j,n), ±6 h (Figure 2c,g,k,o), and ±12 h (Figure 2d,h,l,p) of the satellite over pass time. In Figure 2, the red solid line = regression line, the black solid line = 1:1 line, and the dashed lines = EE envelope. The numbers of coincident observation were increased by increasing time intervals as a maximum number of coincident observations were matched for ±12 h and a minimum number of coincident observations were found for ±2 h. For different time intervals, results showed that the retrieved AOD observations were well correlated with the MAN AOD measurements for ±2 h, has small RMSE for ±12 h, and a large percentage of retrievals within the EE for ±4 h. The DT algorithm underestimates AOD for both low (AOD < 0.4) and high

(AOD > 0.4) aerosol loadings [36] which might be due to large errors in the estimated surface reflectance and aerosol schemes used in look-up-table (LUT) for aerosol retrievals [43]. The performance of the $ODLA_{AOD}$ retrievals was much better than the other SDS in terms of the agreement with the MAN AOD measurements, a large percentage of retrievals within the EE, and small RMSE. The good agreement indicates that the DT10K AOD retrievals followed the actual variations in aerosol concentrations as measured by MAN AOD [68,69]. Overall, the performance of the DT10K algorithm was not satisfactory in terms of data quality as maximum 61% of the retrievals for ±4 h were within the EE, which is less than one standard deviation confidence interval, i.e., about 66% of points should fall within ±EE from the true AOD, which indicates that the DT10K ocean algorithm does not meet the requirements of the EE over the China seas and the eastern Indian Ocean.

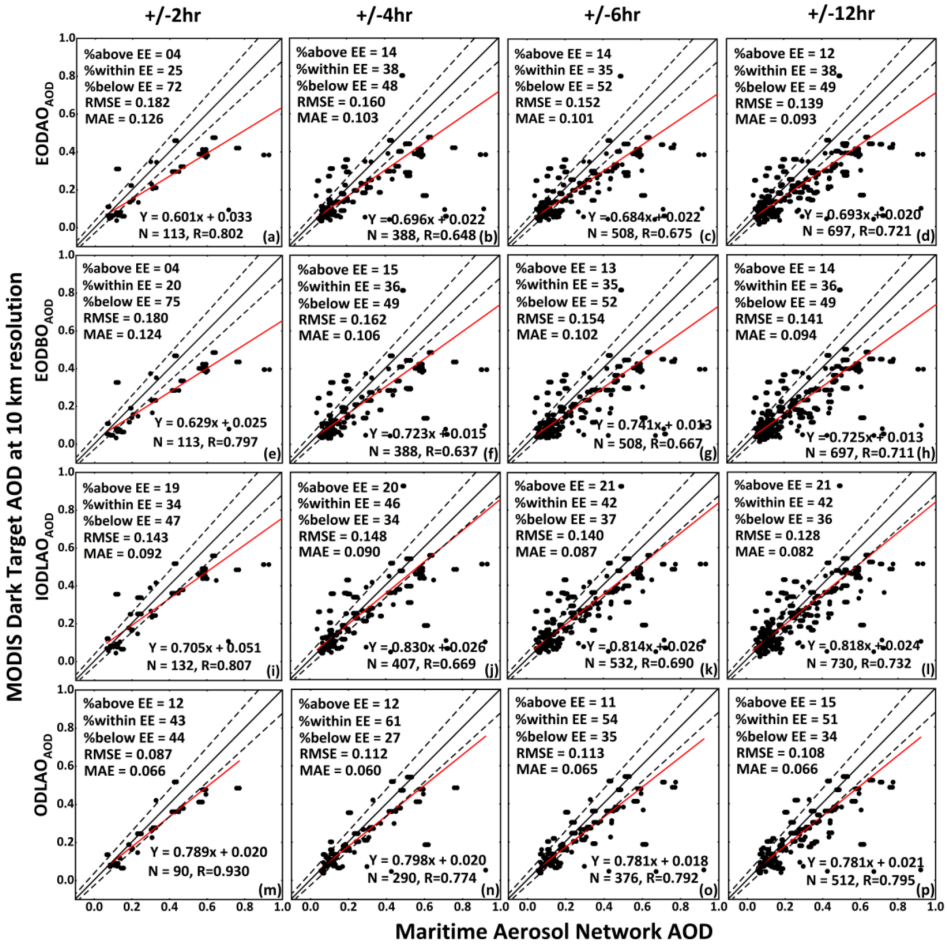


Figure 2. Validation of MODIS DT AOD at 10 km obtained from the SDS Effective_Optical_Depth_Average_Ocean AOD (**a**–**d**), Effective_Optical_Depth_Best_Ocean AOD (**e**–**h**), Image_Optical_Depth_Land_And_Ocean (**i**–**l**), and Optical_Depth_Land_And_Ocean observations (**m**–**p**) against MAN AOD over South China Sea for different time intervals, i.e., ±2 h (**a**,**e**,**i**,**m**), ±2 h (**b**,**f**,**j**,**n**), ±6 h (**c**,**g**,**k**,**o**) and ±12 h (**d**,**h**,**l**,**p**). The black solid line = 1:1 line, the red solid line = regression line, and the dashed black lines = EE bounds.

MAN AOD measurements were not available for winter seasons, therefore seasonal validation of the DT10K AOD observations was conducted for spring, summer, and autumn seasons (Figure 3) using AOD observations obtained from four different SDS for ±12 h of the satellite overpass as for this time intervals, DT10K has large numbers of coincident observations. Larger and small numbers of coincident observations were available for spring and summer, respectively. DT AOD was underestimated for high aerosol loadings during spring and autumn, whereas overestimated

during summer. This was might be due to the regional meteorology and dust aerosol generation and transport for each season [70]. The quality of the $EODAO_{AOD}$ (Figure 3a–c), $EODBO_{AOD}$ (Figure 3d–f), and $IODLAO_{AOD}$ (Figure 3g–i) retrievals were good in spring than summer and autumn, whereas agreement with MAN AOD was not good. All these of AOD retrievals do not meet the requirements of the EE for each season as the percentage within the EE was less than 66%. Good quality and agreement with MAN AOD were observed for $ODLAO_{AOD}$ observations (Figure 3j–l) in summer as the correlation was 0.856 and 75% of the retrievals were within the EE, although only 51 coincident observations were available.

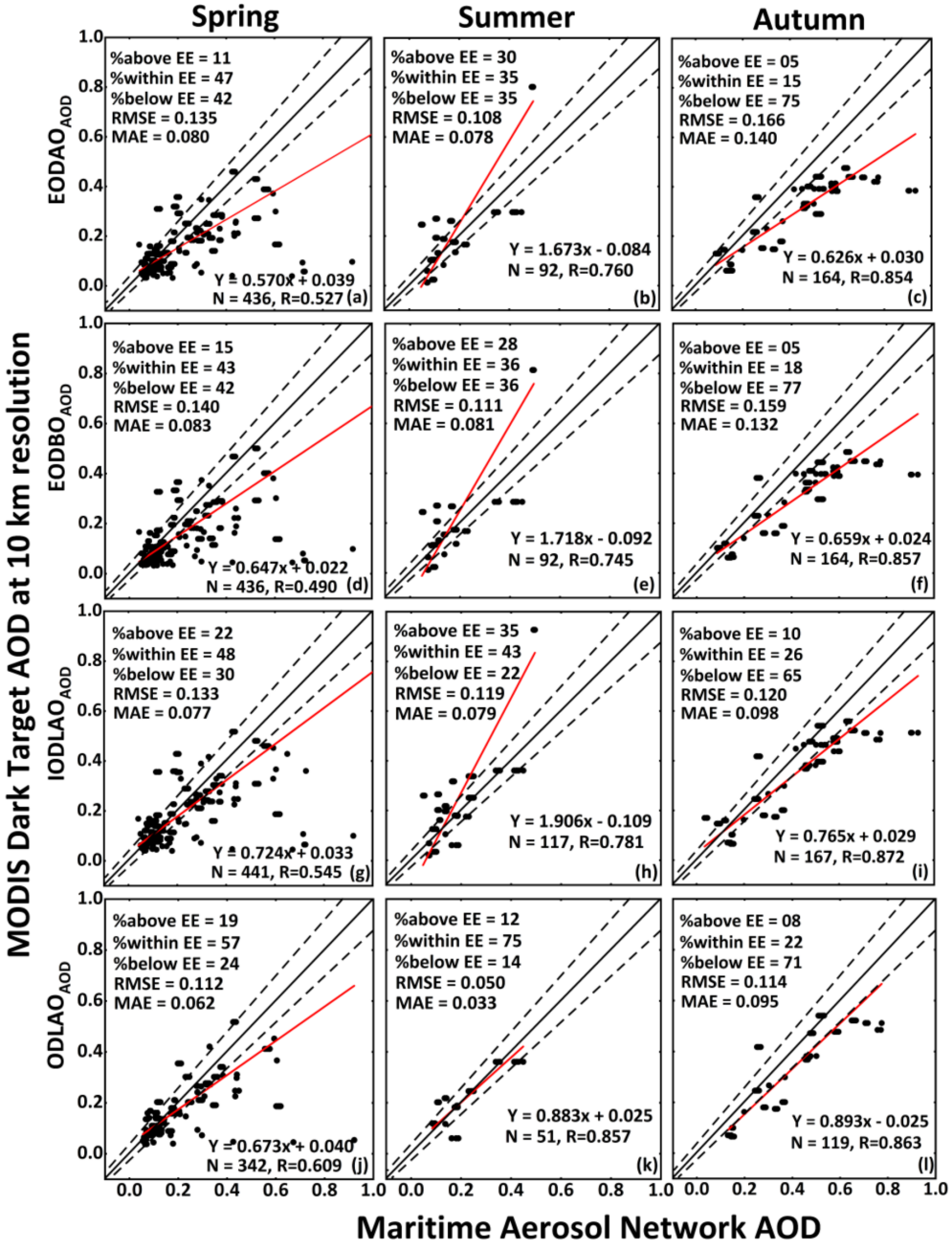


Figure 3. Seasonal validation of MODIS DT $EODAO_{AOD}$ (**a–c**), $EODBO_{AOD}$ (**d–f**), $IODLAO_{AOD}$ (**g–i**), and $ODLAO_{AOD}$ (**j–l**) observations at 10 km resolution. The black solid line = 1:1 line, the red solid line = regression line, and the dashed black lines = EE bounds.

4.1.2. Validation of DT AOD at 3 km Resolution

As with the DT10K, validation of the DT3K $EODAO_{AOD}$ (Figure 4a–d), $EODBO_{AOD}$ (Figure 4e–h), $IODLAO_{AOD}$ (Figure 3i–l), and $ODLAO_{AOD}$ observations (Figure 4m–p) was conducted against MAN AOD measurements over four different time intervals. Similar trends as DT10K was observed in several coincident observations, RMSE, correlation and the percentage of retrievals within the EE. However, the DT3K has a small number of coincident observations than the DT10K for each time interval. For different time intervals, validation showed that the retrieved AOD observations were well correlated with the MAN AOD measurements for ±2 h, shown small RMSE for ±12 h, and a large percentage of retrievals within the EE for ±4 h. The DT3K has large underestimation compared to the DT10K during both low to high pollution episodes which might be caused by an error in the surface reflectance [42,44,45]. The performance of the $ODLA_{AOD}$ retrievals was much better than the other SDS in terms of the agreement with the MAN AOD measurements, a large percentage of retrievals within the EE, and small RMSE. However, the DT3K did not perform well in terms of data quality as maximum 60% of the retrievals for ±4 h were within the EE, which is less than one standard deviation confidence interval, i.e., about 66% of points should fall within ±EE from the true AOD, which indicates that the DT3K ocean algorithm resolution does not meet the requirements of the EE over the South China Sea.

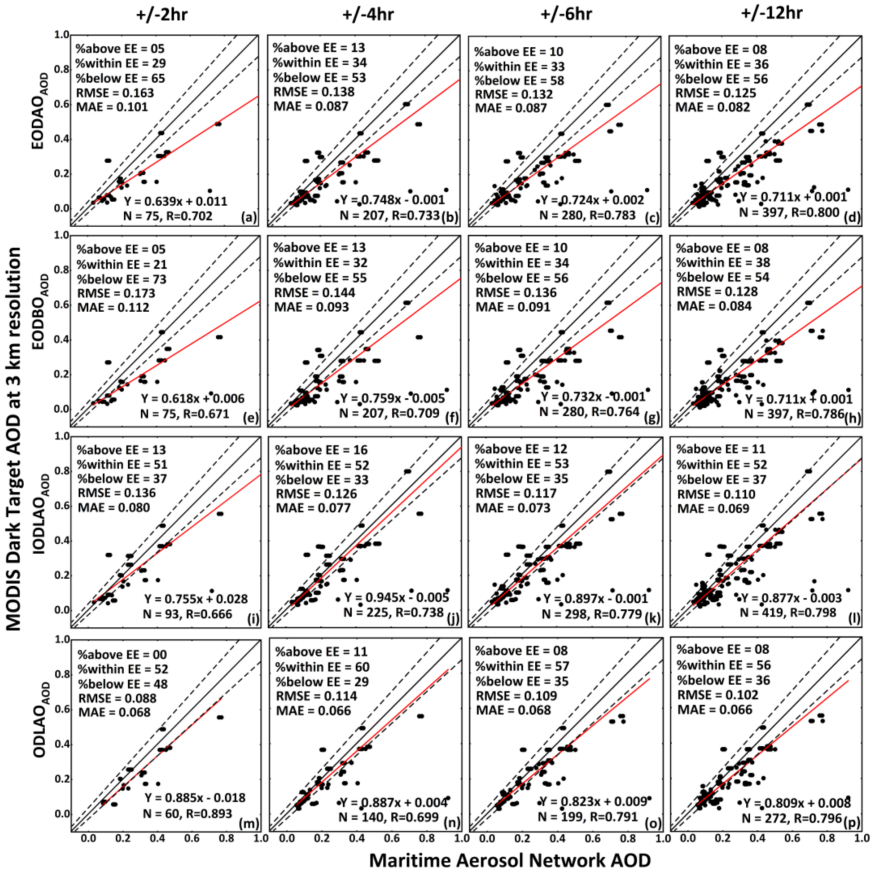


Figure 4. Validation of MODIS DT AOD at 3 km obtained from the SDS Effective_Optical_Depth_Average_Ocean AOD (**a**–**d**), Effective_Optical_Depth_Best_Ocean AOD (**e**–**h**), Image Optical Depth Land And Ocean (**i**–**l**), and Optical Depth Land And Ocean observations (**m**–**p**) against MAN AOD over South China Sea for different time intervals, i.e., ±2 h (**a**,**e**,**i**,**m**), ±2 h (**b**,**f**,**j**,**n**), ±6 h (**c**,**g**,**k**,**o**) and ±12 h (**d**,**h**,**l**,**p**). The black solid line = 1:1 line, the red solid line = regression line, and the dashed black lines = EE bounds.

As with the DT10K algorithm, a large number of coincident observations were available in spring, and large underestimation and RMSE were observed in autumn for each AOD dataset (Figure 5). The DT3K algorithm has less number of coincident observations than the DT10K algorithm but performed well (Figure 5). DT has good quality retrievals, but poorly correlated with MAN measurements during spring than autumn. However, $ODLAO_{AOD}$ observations were well correlated with MAN AOD with large percentage within the EE and small RMSE during the summer season. These are similar findings as the DT10K algorithm.

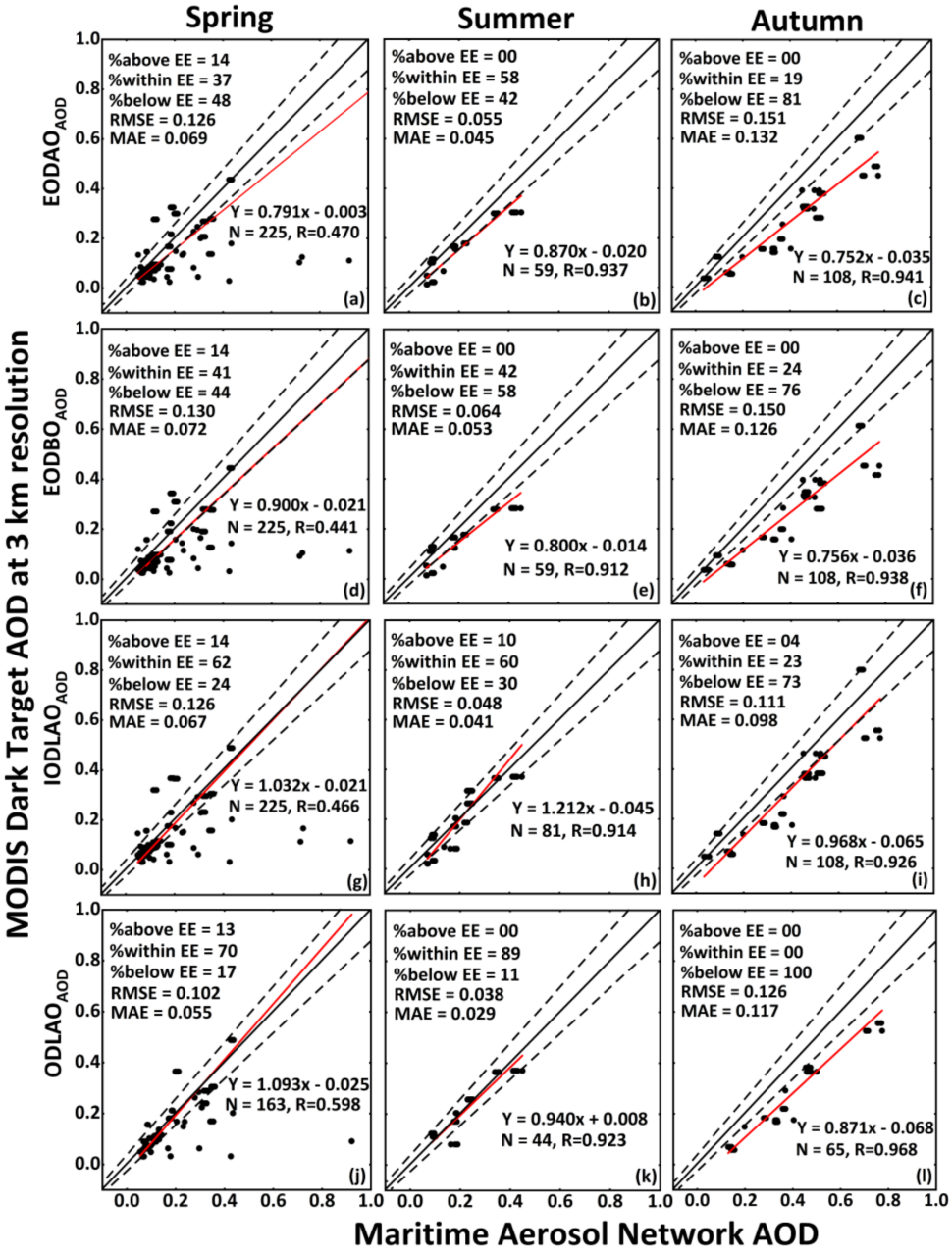


Figure 5. Seasonal validation of MODIS DT $EODAO_{AOD}$ (**a**–**c**), $EODBO_{AOD}$ (**d**–**f**), $IODLAO_{AOD}$ (**g**–**i**), and $ODLAO_{AOD}$ (**j**–**l**) observations at 10 km resolution. The black solid line = 1:1 line, the red solid line = regression line, and the dashed black lines = EE bounds.

4.2. Comparison between DT10K and DT3K

DT3K $EODAO_{AOD}$ (Figure 6a), $EODBO_{AOD}$ (Figure 6b), $IODLAO_{AOD}$ (Figure 6c) and $ODLAO_{AOD}$ (Figure 6d) observations were compared with the DT10K observations for each cruise as shown in Figure 6. Many coincident observations were available for $IODLAO_{AOD}$, and a small number of observations were available for $ODLAO_{AOD}$ which contains only highest quality flag AOD observations. All the parameters of DT3K and DT10K were well correlated with each other with R of 0.94 to 0.99, the slope of 0.92 to 1.02, and RMSE of 0.015 to 0.046. Overall, $ODLAO_{AOD}$ was robust and performed well with highest R of 0.99, slope equal to 1.0 and smallest RMSE 0.015 compared to the other parameters.

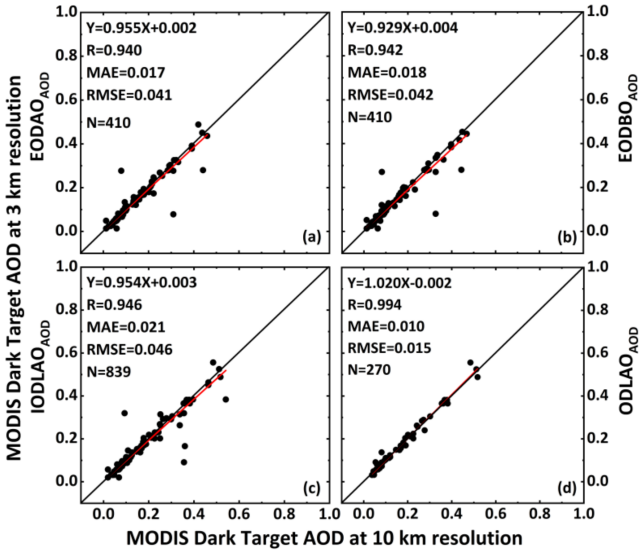


Figure 6. Comparison between MODIS DT3K and DT10K $EODAO_{AOD}$ (**a**), $EODBO_{AOD}$ (**b**), $IODLAO_{AOD}$ (**c**), and $ODLAO_{AOD}$ (**d**) observations.

4.3. Error Analysis

To analyze the errors (MODIS–MAN) in the DT3K and DT10K with respect to seasons over water surfaces, MODIS remote sensing reflectance, which was converted to normalized water reflectance ($Rs = Rrs \times \pi$), was obtained corresponding to each AOD values. Results show that errors in the DT10K (Figure 7) have a less negative correlation with normalized water reflectance than the errors in the DT3K (Figure 8), especially for $EODAO_{AOD}$ (Figures 7a and 8a), $EODBO_{AOD}$ (Figures 7b and 8b), and $IODLAO_{AOD}$ (Figures 7c and 8c) observations. These results indicate that the DT3K mostly underestimates AOD over turbid waters where normalized water reflectances are high and overestimates AOD over clear water where normalized water reflectances are relatively low compared to the DT10K. For example, significant underestimation was observed in spring for high values of normalized water reflectance, and this was might be due to an error in the estimated surface reflectance used in the DT algorithm [43]. This underestimation in the DT3K AOD retrievals was more prominent because some pixels might be retained in the DT3K which are deselected by the DT10K during threshold criteria [44]. It is worth mentioning that $ODLAO_{AOD}$ (Figures 7d and 8d) has a weak correlation with the normalized water reflectance, and the DT algorithm for this parameter is less sensitive to the water quality and under– and over–estimations do not follow the increasing and decreasing trend of normalized water reflectance. These results showed that the $ODLAO_{AOD}$ observations for the highest quality flag are less sensitive to water types and suitable for accurate aerosol monitoring over the China seas and the eastern Indian Ocean compared to the other parameters.

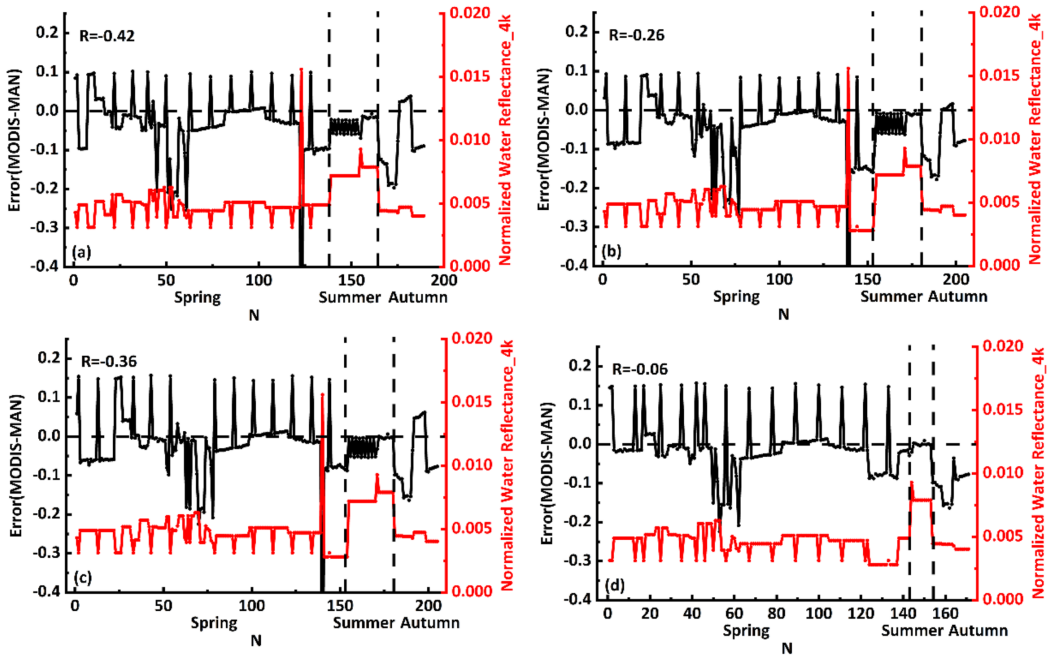


Figure 7. Error (MODIS–MAN) analysis for the DT10K $EODAO_{AOD}$ (**a**), $EODBO_{AOD}$ (**b**), $IODLAO_{AOD}$ (**c**) and $ODLAO_{AOD}$ (**d**) observations using MODIS normalized water reflectance.

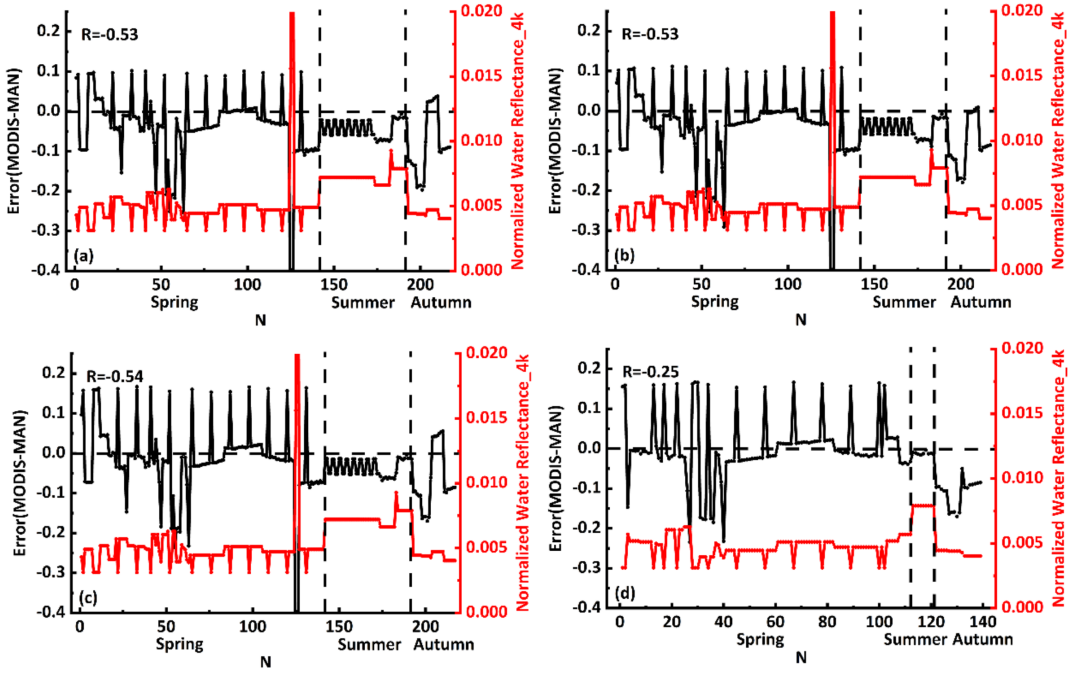


Figure 8. Error (MODIS–MAN) analysis for the DT3K $EODAO_{AOD}$ (**a**), $EODBO_{AOD}$ (**b**), $IODLAO_{AOD}$ (**c**) and $ODLAO_{AOD}$ (**d**) observations using MODIS normalized water reflectance.

5. Conclusions

This study evaluated the MODIS C6 aerosol products based on the DT algorithm at 3 km (DT3K) and 10 km (DT10K) resolutions over the China seas and the eastern Indian Ocean. For this, $EODAO_{AOD}$, $EODBO_{AOD}$, $IODLAO_{AOD}$, and $ODLAO_{AOD}$ observations were obtained from different Scientific Data Sets, i.e., "Effective_Optical_Depth_Average_Ocean", "Effective_Optical_Depth_Best_Ocean",

"Image_Optical_Depth_Land_And_Ocean" and "Optical_Depth_Land_And_Ocean", respectively. For validation, level 1.5 AOD measurements were obtained from the Maritime Aerosol Network (MAN) which were collected using 13 cruises from 2010 to 2014 over the China seas and the eastern Indian Ocean. The MAN AOD data were filtered within (i) ±2 h; (ii) ±4 h; (iii) ±6 h; and (iv) ±12 h of MODIS overpass. This study found that

The DT3K and DT10K algorithm performed equally over the China seas and the eastern Indian Ocean in terms of the agreement with the MAN AOD and percentage of the retrievals within the Expected Error (EE = +(0.04 + 10%), −(0.02 + 10%)),

i. the DT3K coincident AOD observations were less than the DT10K,
ii. a large number of incident observations were available within ±12 h, small RMSE was observed within ±2 h, and a large percentage of the retrievals within the EE was observed within ±4 h,
iii. both the DT3K and DT10K extremely underestimates over water surfaces, and large underestimation being observed during autumn by summer,
iv. the algorithm performed well during summer, but it has fewer numbers of coincident observations for the both DT3K and DT10K,
v. $ODLAO_{AOD}$ observations from the DT3K and DT10K were found better and suitable for use over the China seas and the eastern Indian Ocean compared to the $EODAO_{AOD}$, $EODBO_{AOD}$, and $IODLAO_{AOD}$ in terms of high correlation with the MAN AOD data and large percentage within the EE,
vi. $ODLAO_{AOD}$ observations were less sensitive to the variations in normalized water reflectance, and
vii. overall, this study found that the DT10K and DT3K AOD retrievals do not meet the requirements of the EE as the percentage within the EE was less than 68%.

Acknowledgments: The authors would like to acknowledge NASA Goddard Space Flight Center for MODIS data, and Principle Investigators of MAN sites. We are thankful to Devin White (Oak Ridge National Laboratory) for MODIS Conversion Tool Kit (MCTK). This research was jointly supported by the National Key Research and Development Program of China (No. 2016YFC1400901), the National Natural Science Foundation of China (No. 41576172 and 41506200), the Provincial Natural Science Foundation of Jiangsu in China (No. BK20161532, BK20151526, BK20150914), the National Program on Global Change and Air-sea Interaction (No. GASI-03-03-01-01), a project funded by "the Priority Academic Program Development of Jiangsu Higher Education Institutions (PAPD)".

Author Contributions: Xiaojing Shen performed data processing, analysis and wrote the manuscript; Muhammad designed the study and wrote and modified the manuscript. Zhongfeng Qiu, Deyong Sun, Shengqiang Wang and Weijun Zhu reviewed, provided valuable suggestions, and modified the manuscript.

Conflicts of Interest: The authors declare no conflict of interest. The founding sponsors had no role in the design of the study; in the collection, analyses, or interpretation of data; in the writing of the manuscript, and in the decision to publish the results.

References

1. Solomon, S. IPCC (2007): Climate Change The Physical Science Basis. In *AGU Fall Meeting Abstracts*; Cambridge University Press: Cambridge, UK, 2007.
2. Koren, I.; Altaratz, O.; Remer, L.A.; Feingold, G.; Martins, J.V.; Heiblum, R.H. Aerosol-induced intensification of rain from the tropics to the mid-latitudes. *Nat. Geosci.* **2012**, *5*, 118–122. [CrossRef]
3. Cheung, H.-C.; Wang, T.; Baumann, K.; Guo, H. Influence of regional pollution outflow on the concentrations of fine particulate matter and visibility in the coastal area of southern China. *Atmos. Environ.* **2005**, *39*, 6463–6474. [CrossRef]
4. Pope III, C.A.; Ezzati, M.; Dockery, D.W. Fine-particulate air pollution and life expectancy in the United States. *N. Engl. J. Med.* **2009**, *2009*, 376–386. [CrossRef] [PubMed]
5. Winker, D.; Tackett, J.; Getzewich, B.; Liu, Z.; Vaughan, M.; Rogers, R. The global 3-D distribution of tropospheric aerosols as characterized by CALIOP. *Atmos. Chem. Phys.* **2013**, *13*, 3345–3361. [CrossRef]

6. Holben, B.N.; Eck, T.; Slutsker, I.; Tanre, D.; Buis, J.; Setzer, A.; Vermote, E.; Reagan, J.; Kaufman, Y.; Nakajima, T. AERONET—A federated instrument network and data archive for aerosol characterization. *Remote Sens. Environ.* **1998**, *66*, 1–16. [CrossRef]
7. Holben, B.; Tanre, D.; Smirnov, A.; Eck, T.; Slutsker, I.; Abuhassan, N.; Newcomb, W.; Schafer, J.; Chatenet, B.; Lavenu, F. An emerging ground-based aerosol climatology: Aerosol optical depth from AERONET. *J. Geophys. Res. Atmos.* **2001**, *106*, 12067–12097. [CrossRef]
8. Smirnov, A.; Holben, B.; Slutsker, I.; Giles, D.; McClain, C.; Eck, T.; Sakerin, S.; Macke, A.; Croot, P.; Zibordi, G. Maritime aerosol network as a component of aerosol robotic network. *J. Geophys. Res. Atmos.* **2009**, *114*, 605–617. [CrossRef]
9. Smirnov, A.; Sayer, A.; Holben, B.; Hsu, N.; Sakerin, S.; Macke, A.; Nelson, N.; Courcoux, Y.; Smyth, T.; Croot, P. Effect of wind speed on aerosol optical depth over remote oceans, based on data from the Maritime Aerosol Network. *Atmos. Meas. Tech.* **2012**, *5*, 377. [CrossRef]
10. Herman, M.; Deuzé, J.; Devaux, C.; Goloub, P.; Bréon, F.; Tanré, D. Remote sensing of aerosols over land surfaces including polarization measurements and application to POLDER measurements. *J. Geophys. Res. Atmos.* **1997**, *102*, 17039–17049. [CrossRef]
11. Torres, O.; Bhartia, P.; Herman, J.; Sinyuk, A.; Ginoux, P.; Holben, B. A long-term record of aerosol optical depth from TOMS observations and comparison to AERONET measurements. *J. Atmos. Sci.* **2002**, *59*, 398–413. [CrossRef]
12. North, P.R. Estimation of aerosol opacity and land surface bidirectional reflectance from ATSR-2 dual-angle imagery: Operational method and validation. *J. Geophys. Res. Atmos.* **2002**, *107*. [CrossRef]
13. Torres, O.; Tanskanen, A.; Veihelmann, B.; Ahn, C.; Braak, R.; Bhartia, P.K.; Veefkind, P.; Levelt, P. Aerosols and surface UV products from Ozone Monitoring Instrument observations: An overview. *J. Geophys. Res. Atmos.* **2007**, *112*. [CrossRef]
14. Prados, A.I.; Kondragunta, S.; Ciren, P.; Knapp, K.R. GOES aerosol/smoke product (GASP) over North America: comparisons to AERONET and MODIS observations. *J. Geophys. Res. Atmos.* **2007**, *112*. [CrossRef]
15. Sayer, A.; Hsu, N.; Bettenhausen, C.; Jeong, M.; Holben, B.; Zhang, J. Global and regional evaluation of over-land spectral aerosol optical depth retrievals from SeaWiFS. *Atmos. Meas. Tech.* **2012**, *5*, 2169–2220. [CrossRef]
16. Kahn, R.A.; Gaitley, B.J.; Martonchik, J.V.; Diner, D.J.; Crean, K.A.; Holben, B. Multiangle Imaging Spectroradiometer (MISR) global aerosol optical depth validation based on 2 years of coincident Aerosol Robotic Network (AERONET) observations. *J. Geophys. Res. Atmos.* **2005**, *110*. [CrossRef]
17. Kahn, R.A.; Gaitley, B.J.; Garay, M.J.; Diner, D.J.; Eck, T.F.; Smirnov, A.; Holben, B.N. Multiangle Imaging SpectroRadiometer global aerosol product assessment by comparison with the Aerosol Robotic Network. *J. Geophys. Res. Atmos.* **2010**, *115*. [CrossRef]
18. Hauser, A.; Oesch, D.; Foppa, N.; Wunderle, S. NOAA AVHRR derived aerosol optical depth over land. *J. Geophys. Res. Atmos.* **2005**, *110*. [CrossRef]
19. Riffler, M.; Popp, C.; Hauser, A.; Fontana, F.; Wunderle, S. Validation of a modified AVHRR aerosol optical depth retrieval algorithm over Central Europe. *Atmos. Meas. Tech.* **2010**, *3*, 1255–1270. [CrossRef]
20. Vidot, J.; Santer, R.; Aznay, O. Evaluation of the MERIS aerosol product over land with AERONET. *Atmos. Chem. Phys.* **2008**, *8*, 7603–7617. [CrossRef]
21. Hsu, N.C.; Tsay, S.-C.; King, M.D.; Herman, J.R. Aerosol properties over bright-reflecting source regions. *IEEE Trans. Geosci. Remote Sens.* **2004**, *42*, 557–569. [CrossRef]
22. Hsu, N.C.; Tsay, S.-C.; King, M.D.; Herman, J.R. Deep blue retrievals of Asian aerosol properties during ACE-Asia. *IEEE Trans. Geosci. Remote Sens.* **2006**, *44*, 3180–3195. [CrossRef]
23. Sayer, A.M.; Munchak, L.A.; Hsu, N.C.; Levy, R.C.; Bettenhausen, C.; Jeong, M.J. MODIS Collection 6 aerosol products: Comparison between Aqua's e-Deep Blue, Dark Target, and "merged" data sets, and usage recommendations. *J. Geophys. Res. Atmos.* **2015**, *119*, 13965–13989. [CrossRef]
24. Sayer, A.M.; Hsu, N.C.; Bettenhausen, C.; Jeong, M.J.; Meister, G. Effect of MODIS Terra radiometric calibration improvements on Collection 6 Deep Blue aerosol products: Validation and Terra/Aqua consistency. *J. Geophys. Res. Atmos.* **2016**, *120*. [CrossRef]
25. Xiao, Q.; Zhang, H.; Choi, M.; Li, S.; Kondragunta, S.; Kim, J.; Holben, B.; Levy, R.C.; Liu, Y. Evaluation of VIIRS, GOCI, and MODIS Collection 6 AOD retrievals against ground sunphotometer observations over East Asia. *Atmos. Chem. Phys.* **2016**, *16*, 1255–1269. [CrossRef]

26. Levy, R.; Remer, L.; Kleidman, R.; Mattoo, S.; Ichoku, C.; Kahn, R.; Eck, T. Global evaluation of the Collection 5 MODIS dark-target aerosol products over land. *Atmos. Chem. Phys.* **2010**, *10*, 10399–10420. [CrossRef]
27. Remer, L.A.; Kleidman, R.G.; Levy, R.C.; Kaufman, Y.J.; Tanré, D.; Mattoo, S.; Martins, J.V.; Ichoku, C.; Koren, I.; Yu, H.; et al. Global aerosol climatology from the MODIS satellite sensors. *J. Geophys. Res.* **2008**, *113*, D14S07. [CrossRef]
28. Levy, R.C.; Remer, L.A.; Mattoo, S.; Vermote, E.F.; Kaufman, Y.J. Second-generation operational algorithm: Retrieval of aerosol properties over land from inversion of Moderate Resolution Imaging Spectroradiometer spectral reflectance. *J. Geophys. Res.* **2007**, *112*, D13211. [CrossRef]
29. Bilal, M.; Nichol, J.; Wang, L. New customized methods for improvement of the MODIS C6 Dark Target and Deep Blue merged aerosol product. *Remote Sens. Environ.* **2017**, *197*, 115–124. [CrossRef]
30. Bilal, M.; Nichol, J. Evaluation of the NDVI-Based Pixel Selection Criteria of the MODIS C6 Dark Target and Deep Blue Combined Aerosol Product. *IEEE J. Sel. Top. Appl. Earth Obs. Remote Sens.* **2017**, *10*, 3448–3453. [CrossRef]
31. Salomonson, V.V.; Barnes, W.; Masuoka, E.J. *Introduction to MODIS and an Overview of Associated Activities*; Springer: Berlin/Heidelberg, Germany, 2006; pp. 12–32.
32. Levy, R.C.; Remer, L.A.; Dubovik, O. Global aerosol optical properties and application to Moderate Resolution Imaging Spectroradiometer aerosol retrieval over land. *J. Geophys. Res. Atmos.* **2007**, *112*. [CrossRef]
33. Li, C.; Lau, A.-H.; Mao, J.; Chu, D.A. Retrieval, validation, and application of the 1-km aerosol optical depth from MODIS measurements over Hong Kong. *IEEE Trans. Geosci. Remote Sens.* **2005**, *43*, 2650–2658.
34. Bilal, M.; Nichol, J.E. Evaluation of MODIS aerosol retrieval algorithms over the Beijing-Tianjin-Hebei region during low to very high pollution events. *J. Geophys. Res. Atmos.* **2015**, *120*, 7941–7957. [CrossRef]
35. Bilal, M.; Nichol, J.E.; Bleiweiss, M.P.; Dubois, D. A Simplified high resolution MODIS Aerosol Retrieval Algorithm (SARA) for use over mixed surfaces. *Remote Sens. Environ.* **2013**, *136*, 135–145. [CrossRef]
36. Bilal, M.; Nichol, J.E.; Chan, P.W. Validation and accuracy assessment of a Simplified Aerosol Retrieval Algorithm (SARA) over Beijing under low and high aerosol loadings and dust storms. *Remote Sens. Environ.* **2014**, *153*, 50–60. [CrossRef]
37. Zou, B.; Pu, Q.; Bilal, M.; Weng, Q.; Zhai, L.; Nichol, J.E. High-Resolution Satellite Mapping of Fine Particulates Based on Geographically Weighted Regression. *IEEE Geosci. Remote Sens. Lett.* **2016**, *13*, 495–499. [CrossRef]
38. Bilal, M.; Nichol, J.; Spak, S. A New Approach for Estimation of Fine Particulate Concentrations Using Satellite Aerosol Optical Depth and Binning of Meteorological Variables. *Aerosol. Air Qual. Res.* **2017**, *11*, 356–367. [CrossRef]
39. Livingston, J.; Redemann, J.; Shinozuka, Y.; Johnson, R.; Russell, P.; Zhang, Q.; Mattoo, S.; Remer, L.; Levy, R.; Munchak, L. Comparison of MODIS 3 km and 10 km resolution aerosol optical depth retrievals over land with airborne sunphotometer measurements during ARCTAS summer 2008. *Atmos. Chem. Phys.* **2014**, *14*, 2015–2038. [CrossRef]
40. Zhang, J.; Xin, J.; Zhang, W.; Wang, S.; Wang, L.; Xie, W.; Xiao, G.; Pan, H.; Kong, L. Validation of MODIS C6 AOD products retrieved by the Dark Target method in the Beijing–Tianjin–Hebei urban agglomeration, China. *Adv. Atmos. Sci.* **2017**, *34*, 993–1002. [CrossRef]
41. Levy, R.; Mattoo, S.; Munchak, L.; Remer, L.; Sayer, A.; Patadia, F.; Hsu, N. The Collection 6 MODIS aerosol products over land and ocean. *Atmos. Meas. Tech.* **2013**, *6*, 2989. [CrossRef]
42. Remer, L.; Mattoo, S.; Levy, R.; Munchak, L. MODIS 3 km aerosol product: algorithm and global perspective. *Atmos. Meas. Techn.* **2013**, *6*, 1829. [CrossRef]
43. Bilal, M.; Nazeer, M.; Nichol, J.E. Validation of MODIS and VIIRS derived aerosol optical depth over complex coastal waters. *Atmos. Res.* **2017**, *186*, 43–50. [CrossRef]
44. Nichol, J.; Bilal, M. Validation of MODIS 3 km Resolution Aerosol Optical Depth Retrievals Over Asia. *Remote Sens.* **2016**, *8*, 328. [CrossRef]
45. Munchak, L.; Levy, R.; Mattoo, S.; Remer, L.; Holben, B.; Schafer, J.; Hostetler, C.; Ferrare, R. MODIS 3 km aerosol product: applications over land in an urban/suburban region. *Atmos. Meas. Tech.* **2013**, *6*, 1747–1759. [CrossRef]
46. Kaufman, Y.; Tanré, D.; Remer, L.A.; Vermote, E.; Chu, A.; Holben, B. Operational remote sensing of tropospheric aerosol over land from EOS moderate resolution imaging spectroradiometer. *J. Geophys. Res. Atmos.* **1997**, *102*, 17051–17067. [CrossRef]

47. Tanré, D.; Kaufman, Y.; Herman, M.; Mattoo, S. Remote sensing of aerosol properties over oceans using the MODIS/EOS spectral radiances. *J. Geophys. Res. Atmos.* **1997**, *102*, 16971–16988. [CrossRef]
48. Remer, L.A.; Kaufman, Y.; Tanré, D.; Mattoo, S.; Chu, D.; Martins, J.V.; Li, R.-R.; Ichoku, C.; Levy, R.; Kleidman, R. The MODIS aerosol algorithm, products, and validation. *J. Atmos. Sci.* **2005**, *62*, 947–973. [CrossRef]
49. Leeuw, G.D.; Sogacheva, L.; Rodriguez, E.; Kourtidis, K.; Georgoulias, A.K.; Alexandri, G.; Amiridis, V.; Proestakis, E.; Marinou, E.; Xue, Y. Two decades of satellite observations of AOD over mainland China using ATSR-2, AATSR and MODIS/Terra: data set evaluation and large-scale patterns. *Atmos. Chem. Phys.* **2018**, *18*, 1–33. [CrossRef]
50. Ackerman, S.; Strabala, K.; Menzel, P.; Frey, R.; Moeller, C.; Gumley, L. *Discriminating Clear-Sky from Cloud with MODIS Algorithm Theoretical Basis Document (MOD35), Version 5.0*; NASA Goddard Space Flight Cent.: Greenbelt, MD, USA, 2010.
51. Gao, B.C.; Kaufman, Y.J.; Tanre, D.; Li, R.R. Distinguishing tropospheric aerosols from thin cirrus clouds for improved aerosol retrievals using the ratio of 1.38-μm and 1.24-μm channels. *Geophys. Res. Lett.* **2002**, *29*, 36-1–36-4. [CrossRef]
52. Martins, J.V.; Tanré, D.; Remer, L.; Kaufman, Y.; Mattoo, S.; Levy, R. MODIS cloud screening for remote sensing of aerosols over oceans using spatial variability. *Geophys. Res. Lett.* **2002**, *29*. [CrossRef]
53. Remer, L.; Mattoo, S.; Levy, R.; Heidinger, A.; Pierce, R.; Chin, M. Retrieving aerosol in a cloudy environment: aerosol product availability as a function of spatial resolution. *Atmos. Meas. Tech.* **2012**, *5*, 1823. [CrossRef]
54. Li, R.-R.; Kaufman, Y.J.; Gao, B.-C.; Davis, C.O. Remote sensing of suspended sediments and shallow coastal waters. *IEEE Trans. Geosci. Remote Sens.* **2003**, *41*, 559–566.
55. Hu, J.; Kawamura, H.; Hong, H.; Qi, Y. A review on the currents in the South China Sea: seasonal circulation, South China Sea warm current and Kuroshio intrusion. *J. Oceanogr.* **2000**, *56*, 607–624. [CrossRef]
56. Morton, B.; Blackmore, G. South China Sea. *Mar. Pollut. Bull.* **2001**, *42*, 1236–1263. [CrossRef]
57. Barnes, B.B.; Hu, C. Island building in the South China Sea: detection of turbidity plumes and artificial islands using Landsat and MODIS data. *Sci. Rep.* **2016**, *6*, 33194. [CrossRef] [PubMed]
58. Knobelspiesse, K.D.; Pietras, C.; Fargion, G.S.; Wang, M.; Frouin, R.; Miller, M.A.; Subramaniam, A.; Balch, W.M. Maritime aerosol optical thickness measured by handheld sun photometers. *Remote Sens. Environ.* **2004**, *93*, 87–106. [CrossRef]
59. Eck, T.; Holben, B.; Reid, J.; Dubovik, O.; Smirnov, A.; O'neill, N.; Slutsker, I.; Kinne, S. Wavelength dependence of the optical depth of biomass burning, urban, and desert dust aerosols. *J. Geophys. Res. Atmos.* **1999**, *104*, 31333–31349. [CrossRef]
60. Lee Rodgers, J.; Nicewander, W.A. Thirteen ways to look at the correlation coefficient. *Am. Stat.* **1988**, *42*, 59–66. [CrossRef]
61. Cornbleet, P.J.; Gochman, N. Incorrect least-squares regression coefficients in method-comparison analysis. *Clin. Chem.* **1979**, *25*, 432–438. [PubMed]
62. Deming, W.E. *Statistical Adjustment of Data*; John Wiley & Sons Inc.: New York, NY, USA, 1943.
63. Linnet, K. Performance of Deming regression analysis in case of misspecified analytical error ratio in method comparison studies. *Clin. Chem.* **1998**, *44*, 1024–1031. [PubMed]
64. Stöckl, D.; Dewitte, K.; Thienpont, L.M. Validity of linear regression in method comparison studies: is it limited by the statistical model or the quality of the analytical input data? *Clin. Chem.* **1998**, *44*, 2340–2346. [PubMed]
65. Elahi, E.; Zhang, L.; Abid, M.; Javed, M.T.; Han, X. Direct and indirect effects of wastewater use and herd environment on the occurrence of animal diseases and animal health in Pakistan. *Environ. Sci. Pollut. Res.* **2017**, *24*, 6819–6832. [CrossRef] [PubMed]
66. Elahi, E.; Abid, M.; Zhang, L.; Haq, S.U.; Sahito, J.G.M. Agricultural advisory and financial services; farm level access, outreach and impact in a mixed cropping district of Punjab, Pakistan. *Land Use Policy Int. J. Cover. All Asp. Land Use* **2018**, *71*, 249–260. [CrossRef]
67. Willmott, C.J.; Matsuura, K. Advantages of the mean absolute error (MAE) over the root mean square error (RMSE) in assessing average model performance. *Clim. Res.* **2005**, *30*, 79–82. [CrossRef]

68. Bilal, M.; Qiu, Z.; Campbell, J.R.; Spak, S.; Shen, X.; Nazeer, M. A New MODIS C6 Dark Target and Deep Blue Merged Aerosol Product on a 3 km Spatial Grid. *Remote Sens.* **2018**, *10*, 463. [CrossRef]
69. Bilal, M.; Nazeer, M.; Qiu, Z.; Ding, X.; Wei, J. Global Validation of MODIS C6 and C6.1 Merged Aerosol Products over Diverse Vegetated Surfaces. *Remote Sens.* **2018**, *10*, 475. [CrossRef]
70. Proestakis, E.; Amiridis, V.; Marinou, E.; Georgoulias, A.K.; Solomos, S.; Kazadzis, S.; Chimot, J.; Che, H.; Alexandri, G.; Binietoglou, I. 9-year spatial and temporal evolution of desert dust aerosols over South-East Asia as revealed by CALIOP. *Atmos. Chem. Phys.* **2018**, *18*, 1–35. [CrossRef]



© 2018 by the authors. Licensee MDPI, Basel, Switzerland. This article is an open access article distributed under the terms and conditions of the Creative Commons Attribution (CC BY) license (http://creativecommons.org/licenses/by/4.0/).